14th International Conference on Structural Safety and Reliability - ICOSSAR'25
1-6 June, 2025 - Los Angeles California, USA
R. Ghanem, E. Johnson, S. Masri and A. Olivier (Eds)

RESILIENCE METRIC FOR POST-FLOOD ROAD NETWORK

SMITHA D. KODURU [1], AND VIBHU A. VEMANA[2]

[1]University of Alberta
Donadeo Innovation Centre for Engineering
Edmonton, Alberta, Canada T6G 1H9
smitha@ualberta.ca

[2]University of Calgary & Westmount Charter School
2215 Uxbridge Dr NW,
Calgary, Alberta, Canada T2N 3Z3
Vibhu.Vemana@ucalgary.ca

Key words: Flood resilience, road network, satellite imagery, connectivity indices.

Abstract. In the present work, forty-six urban centers in North America with flood events in the past twenty years were selected for development of post-flood resilience metrics. Public domain high-resolution satellite data from pre-flood event, one year after the flood, and five years after the flood were collected and compared. Public domain machine learning algorithms for object identification were utilized to identify the post-flood pavement condition and functionality of bridges. A set of network connectivity indices were calculated for the pre-flood and post-flood road networks based on the functional status of pavement and other transportation elements. The Resilience index was derived from the change in network indices between post-flood and pre-flood events. The current work provides an approach for estimation of resilience metrics for data scarce locations.

1 INTRODUCTION

The functionality recovery of a road network is one of the critical elements of urban resilience after a flood event. Multiple factors affect the recovery, such as the intensity of the flood event, vulnerability of the critical infrastructure components, socio-economic factors affecting the urban center, and other systemic, administrative, and political issues. To quantify the effect of these factors on the resilience, a metric for road network resilience is the first requirement. If the road network connectivity prior to the flood event along with the connectivity status at different time intervals after the event can be characterized, then a resilience metric for connectivity can be developed. A challenging aspect of such a quantification metric is the extraction of the road network connectivity in a post-flood scenario.

In recent years, there have been multiple deep learning tools developed to extract road networks from high-resolution satellite imagery. Given the recent advances in this digital twinning of the roadways, it is possible to construct the connectivity status of the pre-flood road network using a combination of maps and aerial imagery. Similarly, post-flood road network

connectivity can be extracted using aerial or satellite imagery to identify the status of the pavement, as well as major transportation elements such as bridges and tunnels. Using machine learning and network analysis tools, a consistent network index for the road network connectivity can be established for comparison between the pre- and post-flood road network conditions.

The objective of this study is to identify the public domain machine learning algorithms that can classify the flood status and consequently provide inputs to derive roadway functionality. A second objective is to identify the road network connectivity indices that can be reliably used to indicate network restoration without additional information regarding the roadway capacity, traffic volume, or other usage metrics. The necessity to address these two objectives is described in the next section as the flood resilience framework is presented. The datasets used to address the two objectives of this study are also summarized. Following this, the approach for the acquisition of the satellite imagery and the public domain machine learning algorithms that use image segmentation for flood status identification are described. This is followed by a description for the network connectivity indices and the potential resilience metrics. The study concludes with recommendations for future work based on the network analysis and resilience metrics results, as well as the performance of the public domain image segmentation algorithms.

2 FLOOD RESILIENCE FRAMEWORK

2.1 Methodology

Resilience is defined in the literature as the duration over which the infrastructure functionality is restored following an extreme load event. In the case of road networks subjected to floods, there are multiple resilience metrics proposed in the literature such as restoration of duration of travel, volume of traffic, and multi-dimensional metrics based on user perception such as proximity, availability, adequacy, accessibility, affordability, and awareness [1]. However, evaluating such measures requires detailed information regarding the physical status of road network elements, pre-flood event traffic volumes and speed, land usage, community requirements and post-event community experience. These types of data are not typically available around the world in developing and under-developed nations which are vulnerable not only to the extreme flood events due to the changing climate, but also to the socio-economic impacts of the delayed restoration of road networks.

In the absence of specific data related to road network, infrastructure vulnerability, and recovery activities, an emerging area of research is to use surrogate models to represent climate risks through spatial data as well as to use the satellite-based imagery to track the restoration rate of utilities [2]. Leveraging the public domain spatial data, it is possible to evaluate the correlation between the flood resilience and socio-economic factors at a regional or sub-regional basis. Such indirect measurement approaches help to quickly identify the most vulnerable communities in need of international aid, to prepare for climate risk mitigation, and to develop policies that address socio-economic inequalities exacerbated by the climate hazards.

Figure 1 shows the relationships between the factors affecting the road network resilience. It is noted that in developed nations where infrastructure maintenance and disaster responses are well-planned, direct data-driven approaches can be used to empirically quantify various sub-factors affecting these relationships. For example, in the United States, there are detailed

inventories of the roadway infrastructure elements such as bridges and tunnels, and databases on bridge failures due to flood events [3, 4]. Furthermore, the federal emergency management administration (FEMA) has been mandated to identify the flood risks, provide emergency planning, and oversee disaster assistance [5].

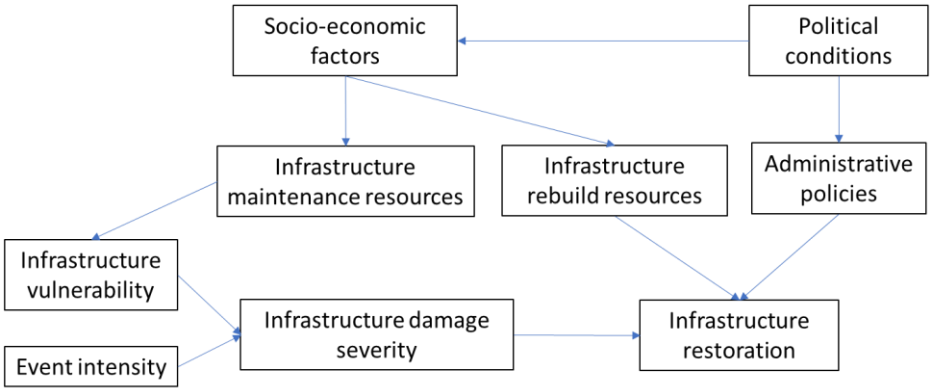

Figure 1: Factors affecting resilience

Figure 2 shows the approach proposed in the present study to identify the relationship between the socio-economic impacts and the disaster resilience. The dotted boxes in the figure show the topics addressed by the objectives of this study. The rest of the components are expected to be addressed in future research.

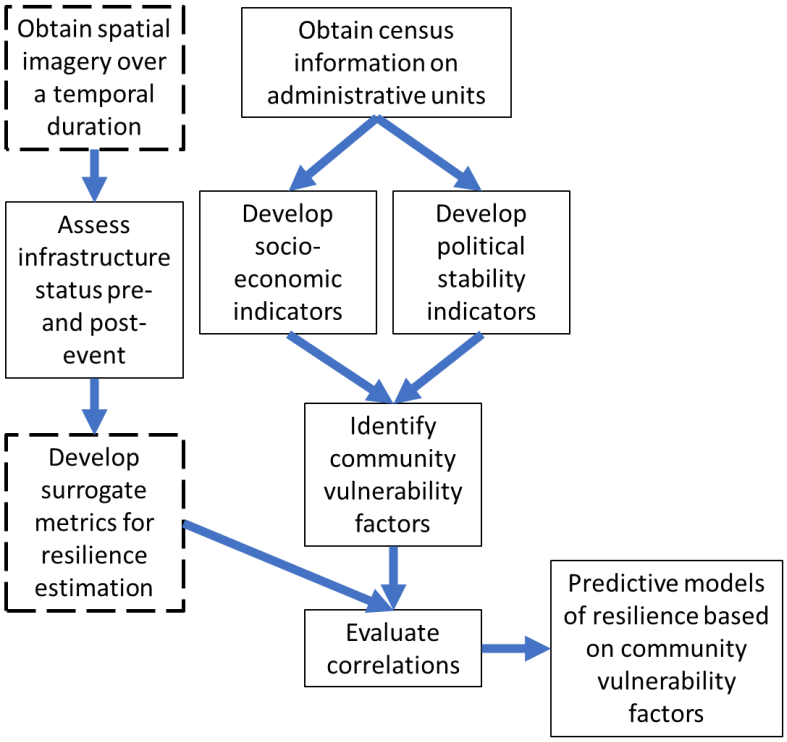

Figure 2: Approach for surrogate analysis of resilience

2.2 Datasets

To develop the tools for acquiring satellite imagery and applying the machine learning approaches for identifying flood status and road network availability, an initial test data set was selected from more than fifty urban centers in the United States. The United States has high-resolution satellite imagery from Landsat satellites over a longer duration as well as independent databases to verify the status of flood events and infrastructure elements [4]. The availability of these multiple independent sources of public domain data enables performance evaluation of the surrogate models.

The urban centers were selected based on the known flood events in the past ten years that had extensive infrastructure impacts. The size of the urban centers varied from approximately 1 sq.km to 400 sq.km and were affected by four major flood events in 2018 and 2019. Three of the flood events were riverine floods in the Midwest while one was due to a hurricane event. The selection of the flood events was also influenced by the data availability from independent sources. Figure 3 shows the location of the 46 urban centers chosen for obtaining the satellite imagery.

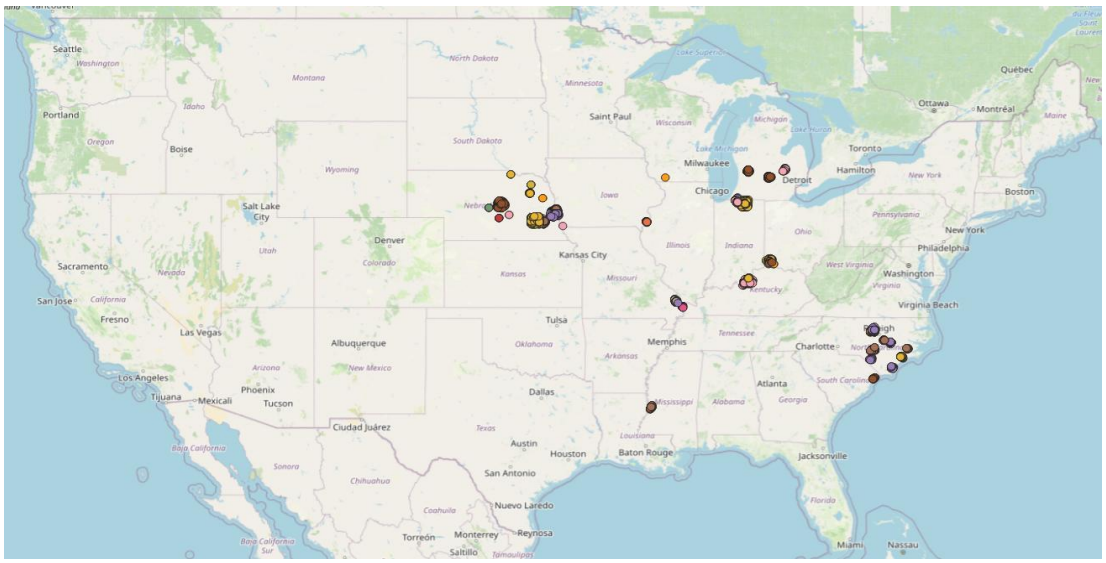

Figure 3: Locations of the urban centers in the dataset

3 SATELLITE IMAGERY

3.1 Acquisition and resolution

High-resolution land imagery was available for the United States from multiple sources such as the National Agriculture Imagery Program (NAIP) [6], the Landsat7 and Landsat8 imagery databases maintained by the United States Geological Survey [7], and the Sentinel 1-2 databases from the Copernicus Programme of the European Space Agency [8]. The satellite imagery was obtained from Sentinel 1-2 databases due to their worldwide coverage and the higher resolution of the Sentinel 2 true-colour images at 10m per pixel compared to the Landsat7/8 true-colour images at 30m per pixel. Sentinel-2 satellite images also have a revisit time of 5 days compared to Landsat-8's 16-day revisit time, which increases the likelihood of capturing the flood

inundation of a location given that the average duration of flood inundation can be less than a week. Furthermore, Sentinel 1-2 are used for the flood monitoring and emergency response of multiple locations in the Europe [9], which enable future comparison of the outcomes of this study with other independent datasets.

Data acquisition was performed through both the Sentinel API and the Earth Engine API from Google [10, 11, 12]. Sentinel API had data availability from October 2016 and provided high-resolution GeoTiff satellite images. Earth Engine API had data availability from a later date, i.e., from March 2017, but provided faster download of high-resolution datasets. To acquire the imagery of an urban center, the extent of the location was defined based on the latitudes and longitudes bounding the location. The image within the bounding box created by the latitude and longitude coordinates was obtained as a true-colour image from the Sentinel bands B2 (blue), B3 (green), and B4 (red). Furthermore, Sentinel product called Scene Classification (SCL) [13], which classifies the images based on the reflectance and the short-wave infrared (SWIR) bands, was used for cloud removal and the identification of water surfaces. Furthermore, the images also used the time-delay integration (TDI) approach, wherein each image is a composite of the land area covered within the bounding box over a time period where Sentinel 2 had multiple passes over the region. This is achieved by preserving the satellite imagery pixels with the earliest time stamp in the observation period and overlaying the blank pixels with the next valid pixel. The composite images in the study were obtained with a maximum observation period of 30 days. In addition to the true-color images, images were also gamma-corrected to adjust for brightness and downloaded for visual verification. Figure 4 shows an example of the gamma-corrected images of the pre-flood and flood within the bounding box area of an urban center. Figure 5 shows an example of the water surface identification using SCL.

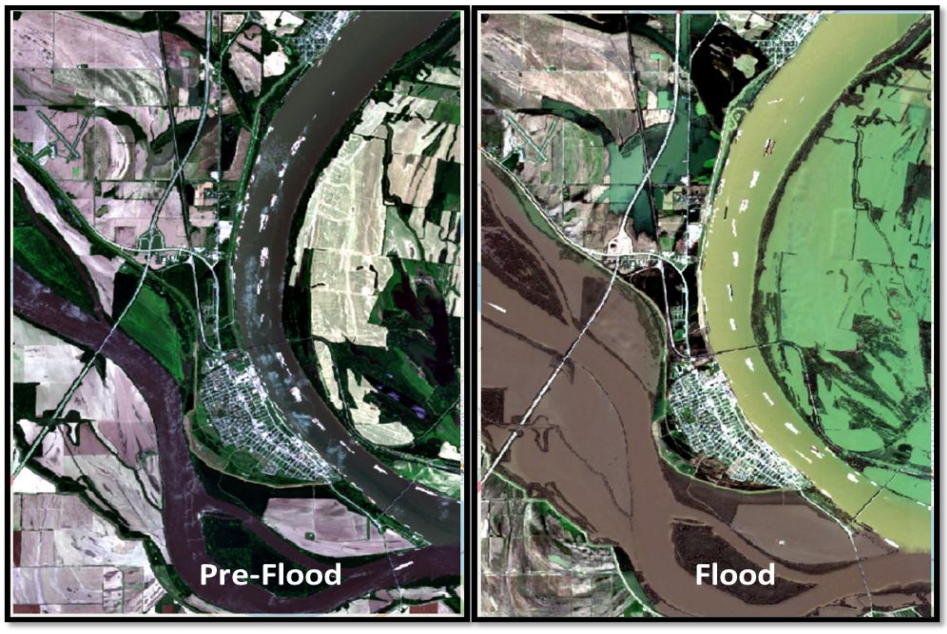

Figure 4: Example of satellite imagery of pre-flood and flood event

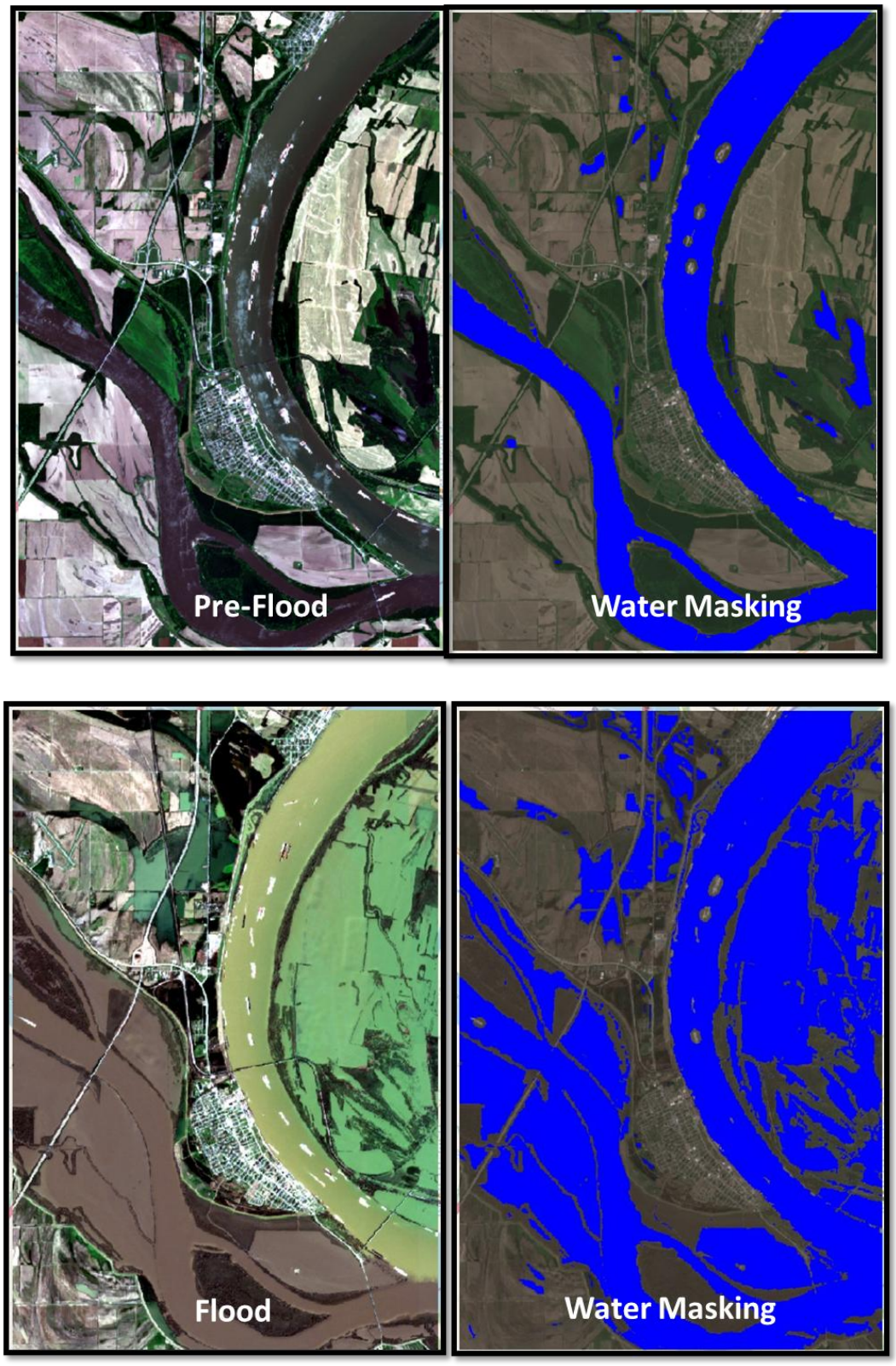

Figure 5: Examples of scene classification to identify water surfaces

3.2 Image segmentation algorithms

To identify the road network affected by a flood event, two different machine learning techniques that use image segmentation are available: 1) to identify the pavement areas and condition and 2) to identify the flood areas based on the surface water. Both approaches have basis in the convolutional neural networks (CNNs) that are routinely used for computer vision and image processing. Although there are multiple deep learning models for road network detection based on image segmentation such as U-Net, SegNet, V-Net, and ResUNet [14], the road network segmentation models specific to flooded roads are not readily available in the public domain.

On the other hand, there are multiple algorithms available for flood detection that use deep learning architectures (e.g., U-Net and SegNet), and transfer learning [15, 16, 17]. It is still challenging for the surface water identification algorithms to be accurate in urban settings to detect minor water surface changes affecting a road network [18]. While one reason could be that the imagery datasets of flooded roads are not extensive, a secondary reason is the challenge in distinguishing the reflectance between the road surface and water surface at the resolution available from the satellite imagery. This challenge prompted development of change detection algorithms using unsupervised learning techniques [19]. However, when the images are generated from time delayed integration, changes to the flood waters within short durations are masked.

In summary, while several public domain machine learning algorithms exist for road network extraction and flood detection through surface water boundary classification, there are no readily available algorithms to identify flood damage to road networks. One approach is to find the geographic intersection of the flood areas with the road network to identify the lost road network elements. However, such approach would need to consider contrasting possibilities, where some road infrastructure elements, such as bridges, may survive the floods intact even if they are intersected by the flood waters, and on the other hand, road infrastructure such highways may lose functionality due to loss of embankment even if the roadway itself is not intersected by the flood waters. An Evaluation of this approach is considered for future research.

4 NETWORK METRICS

4.1 Connectivity indices

Physical road network connectivity can be evaluated using the graph theory measures for connectivity in a planar graph [20]. An alternative approach for resilience estimation is to consider the spatio-temporal demand of particular roadways within the network [21]. While the consideration of traffic flow and demand would provide accurate metrics for the restoration of network functionality, such measures need either detailed traffic flow modelling or an extensive data collection. In the absence of applicable traffic flow models, such as those applicable for mixed traffic flow conditions, and data scarcity of traffic conditions, graph theory measures are quicker to access the overall network connectivity. For this purpose, four network measures are considered in this study. The formulations for the Beta index, Gamma index, Four-way (Fway) index and Eta index are provided in the equations below.

$$Beta = E/V \tag{1}$$

$$Gamma = E/Emax \tag{2}$$

$$Fway = Nf/Nt \tag{3}$$

$$Eta = \sum el/E \tag{4}$$

Where E is the number of edges of the network, V is the number of vertices, $Emax$ is the maximum number of possible edges within the network, Nf is the number of four-way intersections in the network, Nt is the total number of intersections, and el is the length of each edge in the network. Both the Beta and Gamma indices are indirect measures for the proportion of edges in the network. The Fway index is a measure for four-way intersections that assumes that a higher proportion of four-way intersections indicate higher connectivity. The Eta index is an indirect measure of the average edge length and in large networks a substantial loss of roadways is needed to have significant change in Eta.

4.2 Resilience metrics

In this study, two simple resilience metrics were considered based on the direct change to the connectivity indices due to the loss of edges in a graph. These two metrics are expressed as follows:

$$Ri = Ipf/If \tag{5}$$

$$Ri = (Ipf - If)/Ipf \tag{6}$$

Where Ri is the resilience metric, Ipf and If are the network indices computed from post-flood status and pre-flood status, respectively. When the post-flood status is computed at fixed time durations such as one year and five-year periods, the restoration of full network connectivity would be indicated by 1.0 from Equation (5) and by 0.0 from Equation (6).

5 ANALYSIS AND DISCUSSION

5.1 Computation approach

For the 46 urban centers in the dataset, the latitude and longitude coordinates were extracted using the 'FootPrintHandler' function from the BRAILS open-source software [22] and the road network was extracted from the Nominatim API of OpenStreetMap [23]. From the road network, the edges and the nodes of the network were identified using an open-source algorithm from DesignSafe Data Depot [24]. The road network indices for Beta, Gamma, Fway and Eta were computed using the Equations (1-4). Although the satellite imagery of the flood duration was collected for these locations, extraction of the road network status during and after the flood required considerable effort. To demonstrate the comparison of the network index performance, the resilience indices were calculated by assuming that all motorways become non-functional following a flood event, and used that as the post-flood status. Due to nature of disaster response management and funding in the United States, the road network connectivity is typically restored within six months [5]. Therefore, the resilience indices computed from the true post-

flood status wouldn't be informative to evaluate the range of possible values.

Not all the urban centers had motorways, and as such, resilience indices calculated according to Equations (5) and (6) for those locations were either one or zero due to no change in network connectivity. Table 1 shows the list of the 11 urban centers that had zero motorways and the network indices calculated in the pre-flood state. Figure 6 shows the Beta indices for pre-flood and flood status for all the urban centers.

Table 1: List of the urban centers and the pre-flood network indices

City	Beta	Gamma	Fway	Eta
Utica, IN	2.8158	0.9640	0.253968	87.95301
Cold Spring, KY	2.0738	0.6920	0.088819	30.95756
Silver Grove, KY	2.3297	0.7851	0.091667	90.02981
Dannebrog, NE	2.6933	0.9224	0.275862	83.95856
Lynch, NE	2.6800	0.9306	0.368421	134.0932
Broken Bow, NE	3.1304	1.0472	0.452716	81.23929
Randolph, NE	3.1124	1.0499	0.456376	91.14131
Pleasanton, NE	2.7895	0.9636	0.3	92.91693
Valley, NE	2.8354	0.9462	0.278094	539.0144
West Point, NE	3.1037	1.0390	0.434466	97.35921
Louisville, NE	2.6301	0.8889	0.261261	92.17148

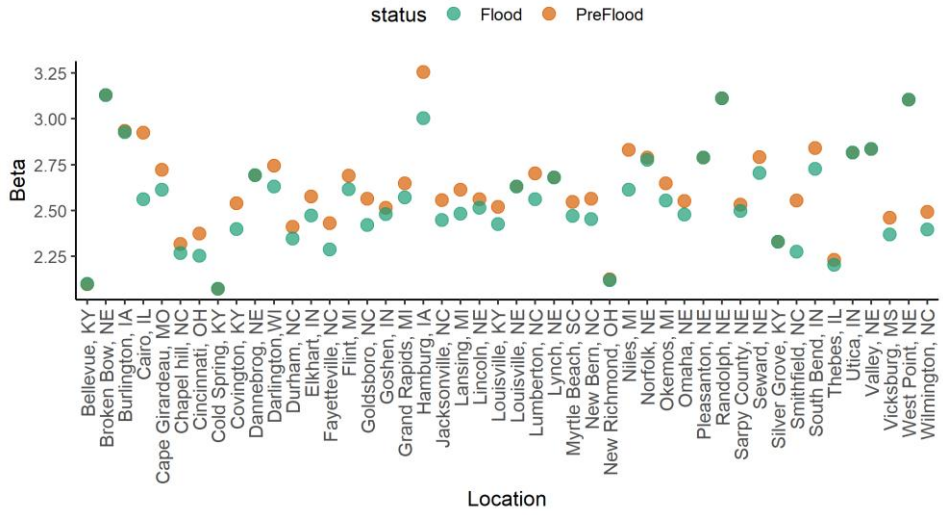

Figure 6: Beta network indices for pre-flood and flood status of 46 cities

5.2 Index comparison

Figure 6 shows a comparison of the network index distributions from pre-flood, i.e., full connectivity status and flood status, which shows the post-flood condition. A wide range of values for a network index would indicate the potential to use it for developing correlations with surrogate factors. Furthermore, the sensitivity of the network index to the change in network connectivity is also a good indicator for its use in calculation of the resilience metric.

In Figure 6, although Fway and Eta, in Figure 6(c) and Figure 6(d) respectively, show a wider range of values within the dataset, the Beta and Gamma indices show a greater sensitivity to the change in network status, as seen in Figure 6(a) and Figure 6(b) respectively. Figure 7 shows the resilience index calculated according to Equation (5) for each connectivity index.

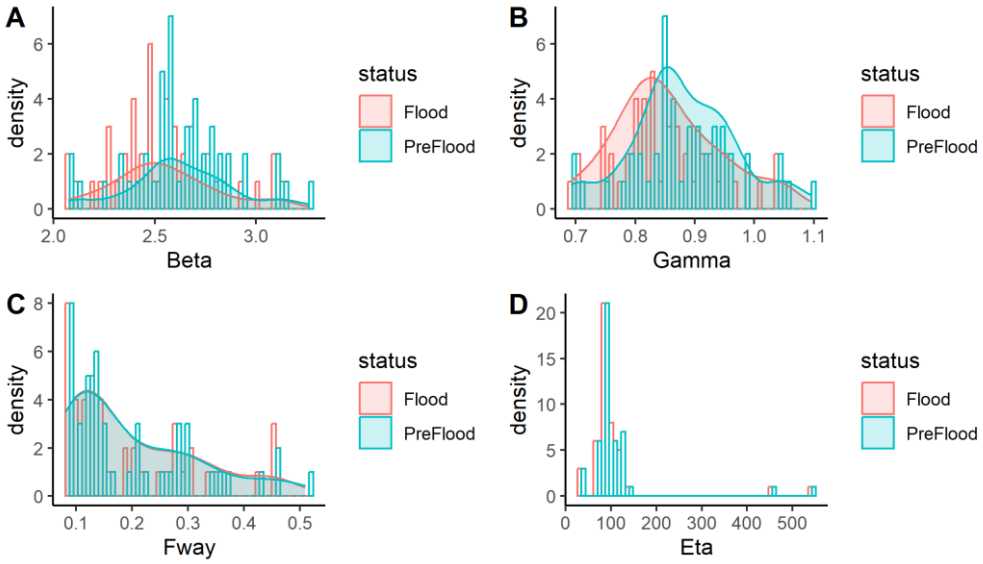

Figure 6: Comparison of network indices for pre-flood and flood status

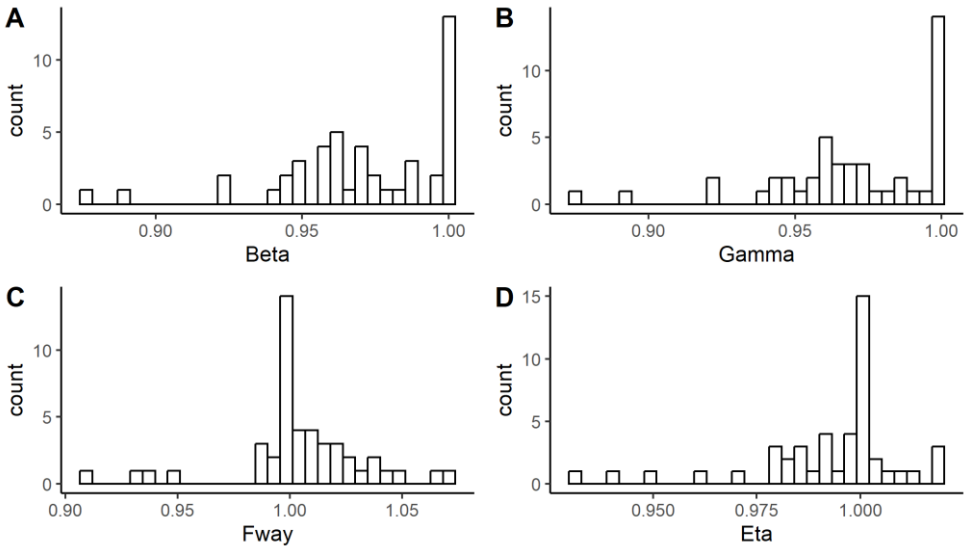

Figure 7: Resilience metric expressed as ratio of connectivity indices

Resilience metrics appear as less than 1.0 when connectivity is not restored for Beta and Gamma, as shown in Figure 7(a) and Figure 7(b), respectively. In contrast, resilience metrics computed using Fway and Eta vary between greater and less than 1.0 and as such, are not reliable indicators for restoration of the network connectivity.

6 FUTURE WORK

The future research would focus on implementation of image segmentation algorithms for road networks and flood detection applied to the satellite imagery, and verify the performance for the prediction of the road network status by independent data sets. When a sufficient dataset size of the flooded road imagery is compiled using a combination of true color, gamma-corrected, and SWIR band images, they will be used for transfer learning with existing image segmentation algorithms.

7 CONCLUSIONS

The contributions of this work are (1) developing a dataset for the application of machine learning approaches to the satellite imagery for identifying post-flood functionality; (2) identifying appropriate network connectivity measures for use as resilience metrics when balanced against data availability, accuracy and uncertainty, and (3) the development of a pathway for automating the resilience estimation of the urban centers across the world, where data collection related to the transportation elements is not as complete as the North American cities. In future, such resilience indices can be correlated with socio-economic factors, and can be used to identify the vulnerability of the urban centers to the cumulative effects of climate change impacts.

REFERENCES

[1] Enderami, S.A., Sutley, E., Helgeson, J. *et al.* Measuring post-disaster accessibility to essential goods and services: proximity, availability, adequacy, and acceptability dimensions. *J Infrastruct Preserv Resil* 5, 12 (2024). https://doi.org/10.1186/s43065-024-00104-0

[2] Best, K., Kerr, S., Reilly, A. *et al.* Spatial regression identifies socioeconomic inequality in multi-stage power outage recovery after Hurricane Isaac. *Nat Hazards* 117, 851–873 (2023). https://doi.org/10.1007/s11069-023-05886-2

[3] *National Bridge Inventory*. (n.d.). https://geodata.bts.gov/datasets/national-bridge-inventory/about

[4] Flint, M. M., Fringer, O., Billington, S. L., Freyberg, D., & Diffenbaugh, N. S. (2017). Historical analysis of hydraulic bridge collapses in the Continental United States. *Journal of Infrastructure Systems*, *23*(3). https://doi.org/10.1061/(asce)is.1943-555x.0000354

[5] The Disaster Relief Fund: Overview and Issues. (2025, April 28). https://www.congress.gov/crs-product/R45484

[6] *National Agriculture Imagery Program - NAIP Hub Site*. (n.d.). https://naip-usdaonline.hub.arcgis.com/

[7] *USGS Landsat 8 Collection 2 Tier 1 Raw Scenes*. (n.d.). Google for Developers. https://developers.google.com/earth-engine/datasets/catalog/LANDSAT_LC08_C02_T1?hl=en

[8] *S2 products*. (n.d.). https://sentiwiki.copernicus.eu/web/s2-products

[9] Drakonakis, G. I., Tsagkatakis, G., Fotiadou, K., & Tsakalides, P. (2022). OmbriaNet—Supervised flood mapping via convolutional neural networks using multitemporal Sentinel-1 and Sentinel-2 data fusion. *IEEE Journal of Selected Topics in Applied Earth Observations and Remote Sensing*, *15*, 2341–2356.

https://doi.org/10.1109/jstars.2022.3155559
[10] *Sentinel-2 datasets in Earth engine*. (n.d.). Google for Developers. https://developers.google.com/earth-engine/datasets/catalog/sentinel-2
[11] *Harmonized Sentinel-2 MSI: MultiSpectral Instrument, Level-2A (SR)*. (n.d.). Google for Developers. https://developers.google.com/earth-engine/datasets/catalog/COPERNICUS_S2_SR_HARMONIZED?hl=en
[12] *Compositing, masking, and mosaicking*. (n.d.). Google for Developers. https://developers.google.com/earth-engine/tutorials/tutorial_api_05?hl=en
[13] *Sentinel-2 L2A*. (n.d.). https://docs.sentinel-hub.com/api/latest/data/sentinel-2-l2a/
[14] Ahmed, M. I., Foysal, M., Chaity, M. D., & Hossain, A. B. M. A. (2023). DeepRoadNet: A deep residual based segmentation network for road map detection from remote aerial image. *IET Image Processing*, *18*(1), 265–279. https://doi.org/10.1049/ipr2.12948
[15] Danish, M. U., Buwaneswaran, M., Fonseka, T., & Grolinger, K. (2024). Graph Attention Convolutional U-NET: a semantic segmentation model for identifying flooded areas. *IECON 2020 the 46th Annual Conference of the IEEE Industrial Electronics Society*, 1–6. https://doi.org/10.1109/iecon55916.2024.10905482
[16] Ghosh, B., Garg, S., & Motagh, M. (2022). AUTOMATIC FLOOD DETECTION FROM SENTINEL-1 DATA USING DEEP LEARNING ARCHITECTURES. *ISPRS Annals of the Photogrammetry, Remote Sensing and Spatial Information Sciences*, *V-3–2022*, 201–208. https://doi.org/10.5194/isprs-annals-v-3-2022-201-2022
[17] Şener, A., Doğan, G. & Ergen, B. A novel convolutional neural network model with hybrid attentional atrous convolution module for detecting the areas affected by the flood. *Earth Sci Inform* 17, 193–209 (2024). https://doi.org/10.1007/s12145-023-01155-9
[18] Shi, L., Yang, K., Chen, Y., & Chen, G. (2024). An interactive prompt based network for urban floods area segmentation using UAV images. *IEEE Journal of Selected Topics in Applied Earth Observations and Remote Sensing*, 1–17. https://doi.org/10.1109/jstars.2024.3498865
[19] Tanim, A. H., McRae, C. B., Tavakol-Davani, H., & Goharian, E. (2022). Flood Detection in Urban Areas Using Satellite Imagery and Machine Learning. *Water*, *14*(7), 1140. https://doi.org/10.3390/w14071140
[20] Soczówka, P., Żochowska, R., & Karoń, G. (2020). Method of the Analysis of the Connectivity of Road and Street Network in Terms of Division of the City Area. *Computation*, *8*(2), 54. https://doi.org/10.3390/computation8020054
[21] Gauthier, P., Furno, A., & El Faouzi, N.-E. (2018). Road Network Resilience: How to Identify Critical Links Subject to Day-to-Day Disruptions. *Transportation Research Record*, *2672*(1), 54-65. https://doi.org/10.1177/0361198118792115
[22] Barbaros Cetiner, Charles Wang, Frank McKenna, SaschaHornauer, Jinyan Zhao, Claudio Perez, & yunhuiguo. (2024). NHERI-SimCenter/BRAILS: Version 3.1.2 (v3.1.2). Zenodo. https://doi.org/10.5281/zenodo.11093530
[23] *Nominatim*. (n.d.). https://nominatim.org/
[24] Agyekum, A., A. Ghavidel, M. Gomez Fuentes, A. Roy, M. Sanger, j. zhao (2024). "Transportation Infrastructure Performance under Seismic Hazards with SimCenter Tools", in Project 8: Transportation Infrastructure Performance under Seismic Hazards with SimCenter Tools [Version 2]. DesignSafe-CI. https://doi.org/10.17603/ds2-b7sj-jr67